Published online 21 June 2018

Nucleic Acids Research, 2018, Vol. 46, No. 15 ***7873–7885***
doi: 10.1093/nar/gky560

Escherichia coli ItaT is a type II toxin that inhibits translation by acetylating isoleucyl-tRNA^{Ile}

Brendan Wilcox[1,†], Ilya Osterman[1,2,†], Marina Serebryakova[1,2], Dmitry Lukyanov[2], Ekaterina Komarova[1,2], Bridget Gollan[3], Natalia Morozova[1,4], Yuri I. Wolf[5], Kira S. Makarova[5], Sophie Helaine[3], Petr Sergiev[1,2], Svetlana Dubiley[1,6], Sergei Borukhov[7,*] and Konstantin Severinov[1,6,8,*]

[1]Centre for Life Sciences, Skolkovo Institute of Science and Technology, Skolkovo 143025, Russia, [2]Lomonosov Moscow State University, A.N. Belozersky Institute of Physico-Chemical Biology, Moscow 119992, Russia, [3]MRC Centre for Molecular Bacteriology and Infection, Flowers Building, Armstrong Road, Imperial College London, London SW7 2AZ, UK, [4]Peter the Great St. Petersburg State Polytechnic University, St. Petersburg, Russia, [5]National Center for Biotechnology Information, National Library of Medicine, Bethesda, MD 20894, USA, [6]Institute of Gene Biology of the Russian Academy of Sciences, Moscow 119334, Russia, [7]Department of Cell Biology, Rowan University School of Osteopathic Medicine at Stratford, Stratford, NJ 08084-1489, USA and [8]Waksman Institute for Microbiology, Rutgers, The State University of New Jersey, Piscataway, NJ 08854, USA

Received April 27, 2018; Revised June 03, 2018; Editorial Decision June 05, 2018; Accepted June 07, 2018

ABSTRACT

Prokaryotic toxin–antitoxin (TA) modules are highly abundant and are involved in stress response and drug tolerance. The most common type II TA modules consist of two interacting proteins. The type II toxins are diverse enzymes targeting various essential intracellular targets. The antitoxin binds to cognate toxin and inhibits its function. Recently, TA modules whose toxins are GNAT-family acetyltransferases were described. For two such systems, the target of acetylation was shown to be aminoacyl-tRNA: the TacT toxin targets aminoacylated elongator tRNAs, while AtaT targets the amino acid moiety of initiating tRNA^{Met}. We show that the *itaRT* gene pair from *Escherichia coli* encodes a TA module with acetyltransferase toxin ItaT that specifically and exclusively acetylates Ile-tRNA^{Ile} thereby blocking translation and inhibiting cell growth. ItaT forms a tight complex with the ItaR antitoxin, which represses the transcription of *itaRT* operon. A comprehensive bioinformatics survey of GNAT acetyltransferases reveals that enzymes encoded by validated or putative TA modules are common and form a distinct branch of the GNAT family tree. We speculate that further functional analysis of such TA modules will result in identification of enzymes capable of specifically targeting many, perhaps all, aminoacyl tRNAs.

INTRODUCTION

Toxin–antitoxin (TA) genes pairs are highly abundant in bacterial and archaeal genomes (1,2). A TA pair consists of proteinaceous toxin and a cognate antitoxin, which can be either an RNA or a protein (3). Based on the nature of antitoxin and the way it counteracts the action of cognate toxin, TA systems are classified into six types (3), of which the type II systems are so far the most extensively studied. Type II antitoxins are proteins which forms a tight complex with their cognate toxins, thereby blocking toxin activity. It is generally accepted that antitoxins are less stable than toxins, especially under stress conditions. Degradation of antitoxin by cellular proteases releases the active toxin (4). The biological function of TA modules is not always clear. Substantial experimental evidence exists for participation of some toxins in plasmid and unstable genomic loci maintenance (5), where they act as selfish 'addiction' modules. Toxin activation can also benefit the host leading, for example, to the suicide of cells infected by bacteriophage (abortive infection), which limits the spread of the virus in a clonal population (6). Some data also point towards the importance of toxin–antitoxin modules for virulence and persistence/antibiotic tolerance (7), although the actual mechanisms are subject of debate and ongoing research.

*To whom correspondence should be addressed. Tel: +1 848 445 6086; Fax: +1 848 445 5735; Email: severik@waksman.rutgers.edu
Correspondence may also be addressed to Sergei Borukhov. Tel: +1 856 566 6271; Fax +1 856 566 6965; Email: borukhse@rowan.edu
†The authors wish it to be known that, in their opinion, the first two authors should be regarded as Joint First Authors.

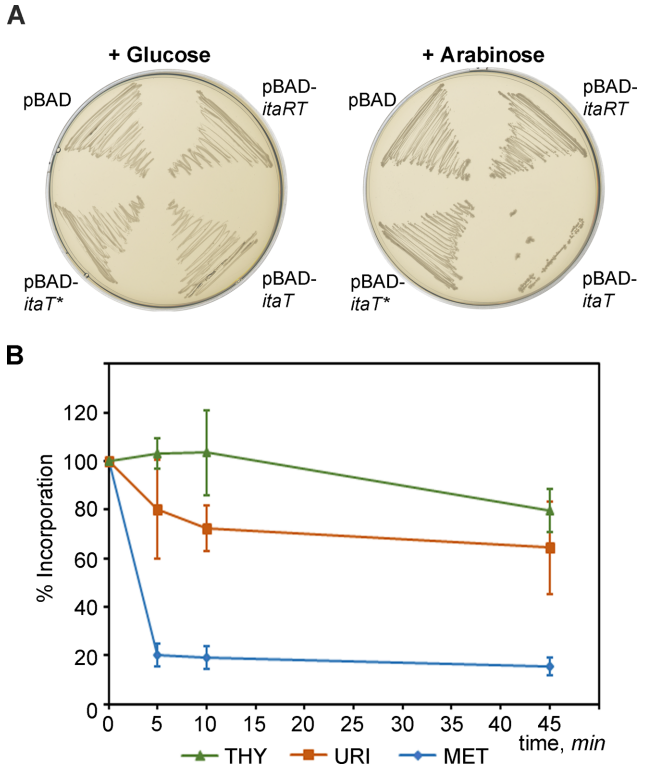

Figure 1. Expression of *itaT* inhibits cell growth by impairing protein synthesis. (**A**) Growth on LB agar plates of *E. coli* MG1655 strain transformed with pBAD33 control vector (pBAD) or the same plasmid expressing the *itaRT* module, *itaT* or *itaT* (itaT*-Y150A mutant). Cells were grown under non-inducing (0.2% glucose) and inducing (20 mM arabinose) conditions as indicated. (**B**) Pulse-labeling of *E. coli* MG1655 cells harboring pBAD33-*itaT* plasmid grown on minimal medium supplemented with arabinose and one of the radiolabeled precursors: [^{3}H]-thymidine (THY), [^{3}H]-uridine (URI) or [^{35}S]-methionine (MET). Incorporation of the radioactivity into DNA, RNA, and protein is normalized to OD_{450} in each sample at 0, 5, 10 and 45 min of induction. The graph shows the percentage of normalized incorporation relative to that before the induction. Error bars in (B) and (D) indicate standard deviation from three independent experiments (see Materials and Methods for details).

Type II toxins target diverse essential biosynthetic pathways of bacteria such as cell wall synthesis, DNA replication and protein translation (8). Interference with normal cell metabolism can be achieved either through physical destruction or reversible modification of targets. Among the validated targets of type II toxins are DNA gyrase, aminoacyl-tRNA synthetases, EF-TU and site-specific cleavage of free or ribosome-bound mRNA, tRNA, or rRNA (9). This list is by no means complete, as bioinformatics surveys continue to identify novel, putative TA modules, most of which remain uncharacterized (10,11). Recently, a new class of type II toxins belonging to GCN5-related (GNAT) superfamily of *N*-acetyltransferases was characterized. Toxins from *Salmonella* Typhimurium were shown to inhibit translation through acetylation of multiple elongator aminoacyl-tRNAs (12,13). Another translational inhibitor, the AtaT toxin from *Escherichia coli* O157:H7, was shown to specifically acetylate the amino group of initiator Met-tRNA^{fMet} preventing its interaction with IF2·GTP (14,15). Toxicity of several other GNAT type II toxins has been demonstrated although their actual targets remain unknown (12,14,16–20).

In this work, we describe a new *itaRT* type II toxin–antitoxin module from *E. coli* HS. The ItaT toxin forms a tight complex with the ItaR antitoxin, and this complex represses transcription of the *itaRT* operon. ItaT is a Gcn5 family acetyltransferase protein. It inhibits protein synthesis by acetylation of charged tRNA. Unlike previously described tRNA-acetylating toxin AtaT, ItaT specifically acetylates both isoaccepting elongator Ile-tRNA^{Ile}s. Our results expand the repertoire of targets of type II acetyltransferase toxins. Computational analysis indicates that toxins of this type are both numerous and diverse, suggesting that additional specificities may be found in nature.

MATERIALS AND METHODS

Plasmid construction

Escherichia coli DH5α was used for cloning. All primers were synthesized by Evrogen (Russia); their sequences are listed in Supplemental Table S1. PCR-amplification was carried out using Phusion DNA polymerase (Thermo Fisher Scientific, USA). To construct plasmids for *in vivo* phenotypic assays, the *itaRT* module, *itaR* and *itaT* genes were PCR-amplified from *E. coli* HS genomic DNA with primers ItaR_F and ItaT_R, ItaR_F and ItaR_R, ItaT_F and ItaT_R, respectively. The PCR products were digested with KpnI and HindIII and inserted under the same sites into a pBAD33 vector containing an arabinose-inducible promoter, creating plasmids pBAD-*itaRT*, pBAD-*itaR*, pBAD-*itaT*. The *itaT-Y150A* mutant (*itaT**) was obtained by site-directed mutagenesis using overlap–extension PCR (21) on an *itaT* DNA template with a combination of ItaTY_F and ItaTY_R primers together with universal pBAD-Forward and pBAD-Reverse primers. The mutant *itaRT** module was obtained similarly using the *itaRT* module as a template. The PCR products were digested with KpnI and HindIII and inserted into pBAD33, creating plasmids pBAD-*itaRT*, pBAD-*itaR*, pBAD-*itaT** and pBAD-*itaRT**.

To construct a plasmid for tandem affinity purification of ItaRT complex, a two-step procedure was used. First, a Strep-tag was introduced into a pET22b vector (Novagen-Millipore, USA). For this, the phosphorylated self-complementary oligonucleotides ST_U and ST_D were annealed and inserted into pET22b digested with NdeI and BamHI, resulting in pET22-strep-his vector. Then, the *itaRT* module was PCR-amplified with Ita_FB and Ita_RX primers and inserted into pET22-strep-his between BamHI and XhoI, resulting in pET22-strep-*itaRT*-his. To construct a plasmid for ItaT purification, the *itaRT* module was first PCR-amplified using Ita_FB and Ita_RXS primer. Then, the PCR product was digested with BamHI and XhoI and ligated into pETDuet-1 vector (Novagen-Millipore, USA) cut with the same enzymes to create pET-his-*itaRT* plasmid.

To construct a transcriptional fusion reporter plasmid for analysis of the regulatory function of ItaR-ItaT complex, the 5′-UTR region of *itaRT* module spanning from position −183 to −11 relative to the expected transcription start site containing putative promoter was amplified with ItaPF

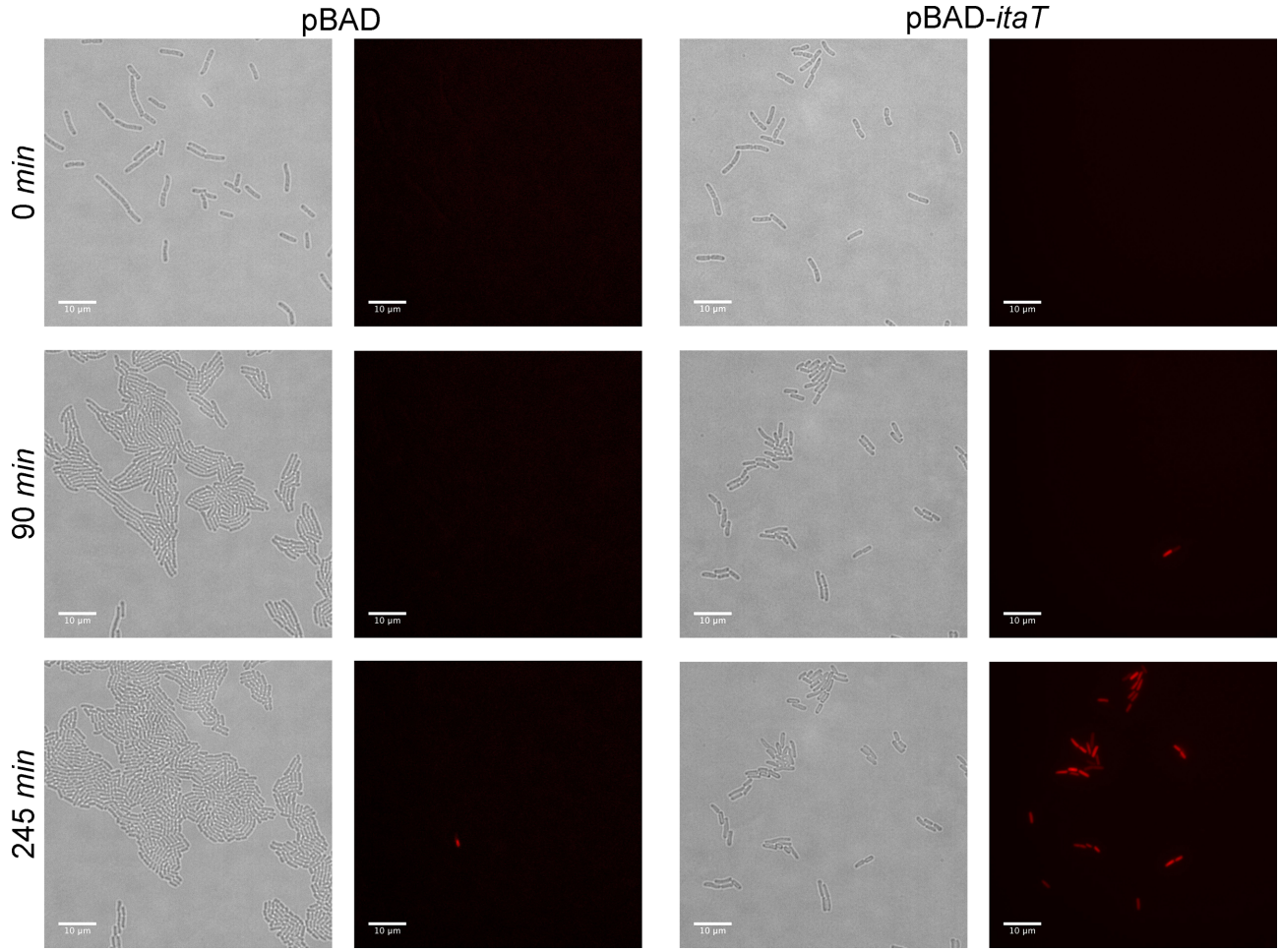

Figure 2. ItaT overproduction leads to cessation of cell growth and affects membrane permability. Time-lapse microscopy of *E. coli* MG1655 cells harboring pBAD33 control plasmid (left two columns) or pBAD33-*itaT* plasmid (right two columns) growing on LB-agarose blocks in the presence of 10 mM arabinose and propidium iodide. Transmitted light and fluorescent microscopy images are shown.

and ItaPR primers. The resulting PCR product was digested with EcoRI and EcoRV and inserted into pFD51-*galK* (22) at the same sites to create pFD-P_{itaRT}-*galK*.

Rates of protein, DNA and RNA synthesis

Escherichia coli MG1655 cells harboring pBAD33-*itaT* were grown at 37°C in 50 ml of M9 minimal media containing a mixture of 19 amino acids without methionine to OD_{450} = 0.4. Cells were then divided into two 25 ml-cultures and grown at 37°C with aeration in the absence or presence of 20 mM arabinose. 500 μl-aliquots before the induction and 5, 10 and 45 min after induction were taken and mixed with 25 μl of solution containing 1 μCi of L-[^{35}S]-methionine (1135 Ci/mmol), 2.5 μCi [methyl-^{3}H]-thymidine (6.7 Ci/mmol), or 2.5 μCi [5-^{3}H]-uridine (20 Ci/mmol) (Perkin-Elmer, USA) supplemented with 10 ng/ml of unlabeled L-methionine, thymidine or uridine, respectively. The pulse-labeling was carried out for 2 min at 37°C on a shaker, and incorporation of radioactive isotopes was halted by the addition of 100 μl of 40% TCA. Samples were transferred onto glass microfiber filters (Whatman, USA), filters were successively washed with 2 ml of 10% TCA and 2 ml of ice-cold ethanol. The radioactivity of insoluble material trapped on filters was measured in a liquid scintillation counter LS60001C (Beckman Coulter, USA). Incorporation of the radioactivity into DNA, RNA and protein is normalized to OD_{450} in each sample at 0, 5, 10 and 45 min of induction. The 100% incorporation corresponds to the value of relative radioactivity observed in samples before the induction (at 0 min).

Regulation of *itaRT* expression assay

Escherichia coli HB101 cells harboring promoterless reporter pFD51-*galK* or transcriptional fusion reporter pFD-P*itaRT-galK* were co-transformed with pBAD-*itaR*, pBAD-*itaT,* pBAD-*itaRT,* or an empty vector pBAD33. Cells were grown in LB media supplemented with ampicillin (50 μg/ml), chloramphenicol (35 μg/ml) and 10 mM arabinose until OD_{600} = 0.6. Cells were harvested by centrifugation, and total RNA was extracted using acid-phenol RNA extraction method. One μg of total RNA was treated with DNase and reverse-transcribed using Maxima First Strand cDNA Synthesis Kit (Thermo Fisher Scientific, USA) with random hexamer primer. The subsequent qPCR analysis of

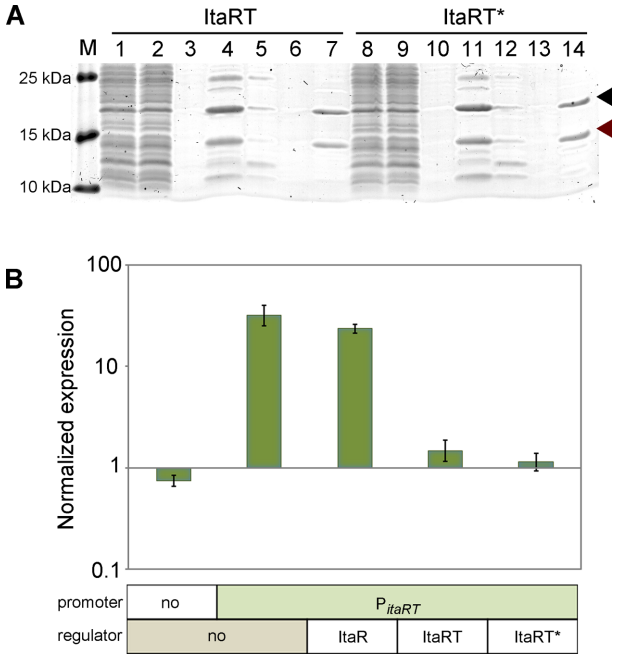

Figure 3. ItaR and ItaT form a stable complex which represses transcription from *itaRT* promoter independent from the ItaT acetylating activity. (**A**) Tandem affinity purification of 6xHis-tagged ItaR co-expressed with Strep-tagged ItaT (left panel, lanes 1–7) or with Strep-tagged ItaT* (right panel, lanes 8–14). Samples separated on Talon Co^{2+}-chelating (lanes 1–4 and 8–11) agarose and Strep-Tactin agarose (lanes 5–7 and 12–14) were analyzed by SDS-PAGE followed by Coomassie staining. Lanes 1–4 and 8–11 represent the initial cell lysates, unbound material, wash fractions and the eluates from Talon resin, respectively. Lanes 5–7 and 12–13 represent the unbound material, wash fractions and the eluates from Strep-Tactin resin, respectively. Lane M shows the molecular weight markers. Black and red arrowheads on the right indicate positions of the ItaT and ItaR protein bands, respectively. (**B**) RT-qPCR analysis of the relative expression of the *galK* transcript in *E. coli*. Transcriptional fusion reporter plasmid pFD-P_{itaRT}-*galK* carrying *galK* under a putative P_{itaRT} promoter or in a promoterless construct (pFD-*galK*) were co-transformed with an empty vector pBAD33, or plasmids expressing ItaR (pBAD-ItaR), co-expressing ItaR and ItaT (pBAD-ItaRT), or ItaRT* (pBAD-ItaRT*). The bars show the relative *galK* expression level (in log scale) normalized to the level of *bla* transcript expressed from the same plasmid. Error bars indicate standard deviation obtained from three independent measurements.

bla and *galK* cDNAs was carried out using Maxima SYBR Green/ROX qPCR Master Mix (Thermo Fisher Scientific) and respective pairs of primers: Amp_F with Amp_R or Gal_F with Gal_R. Absolute quantification (standard curve method) was applied to calculate the expression levels. The standard curves for *bla* and *galK* DNAs were obtained using serial dilutions of the pFD51 plasmid. The resulting *galK* expression level was normalized to the expression level of *bla* gene.

Microscopy

Escherichia coli MG1655 cells harboring pBAD33 or pBAD-*itaT* were grown in LB to an OD_{600} = 0.5. An aliquot of the cell culture was transferred to LB-1.5% agarose block supplemented with 0.2% glucose or 10 mM arabinose, and 20 nM propidium iodide (Sigma-Aldrich, USA) and placed into a microscope chamber of Nikon Ti-E inverted microscope. Two agarose blocks can fit into one microscope chamber enabling simultaneous monitoring of cell growth of induced and uninduced cultures (23). To observe cell recovery after brief induction of ItaT expression, *E. coli* MG1655 cells carrying pBAD-*itaT* were grown to an OD_{600} = 0.5, induced by the addition of 10 mM arabinose, and allowed to grow for additional 30 min at 37°C. Cells were harvested by centrifugation, resuspended in fresh LB containing 0.2% glucose and 20 nM propidium iodide, transferred to LB–1.5% agarose and placed into the microscope chamber for time-lapse observations. The microscope was equipped with Andor's Zyla 4.2 sCMOS camera, Semrock mCherry-40LP filter set for propidium iodide fluorescence detection and custom-made incubation system to maintain cells at 37°C. Image analyses were performed using Fiji-ImageJ software package (24).

Protein expression and purification

ItaRT tandem affinity chromatography. *Escherichia coli* BL21(DE3) cells carrying pET22-strep-*itaRT*-his plasmid were grown to OD_{600} of ∼0.6 in 20 ml of LB medium containing ampicillin (50 μg/ml). Protein expression was induced with 1 mM isopropyl-β-D-thiogalactopyranoside (IPTG), followed by growth at 18°C for 16 h. Cells were harvested by centrifugation, washed with BW buffer (20 mM Tris–HCl, pH 8.0; 300 mM NaCl) and resuspended in 2 ml of BW buffer supplemented with 0.2 mM phenylmethanesulfonyl fluoride (PMSF), 1 mg/ml lysozyme, and 1 mM β-mercaptoethanol. The cells were lysed by sonication, and the debris was removed by centrifugation. The clarified cell lysate was mixed with 100 μl of Talon CellThru Co^{2+}-chelating resin (Takara-Clontech, USA) pre-equilibrated with BW buffer and incubated with gentle rotation at 4°C for 2 h. The resin was washed with BW buffer, and the ItaRT complex was eluted with 1 ml of EB buffer (50 mM Tris–HCl, pH 8.0; 0.5 M imidazole, 300 mM NaCl). The eluted material was combined with 100 μl of Strep-Tactin Superflow Plus resin (Qiagen, USA) and incubated with gentle rotation at 4°C for 4 h. The resin was washed with BW buffer and eluted with 1 ml of BW buffer containing 2.5 mM desthiobiotin (Sigma-Aldrich, USA). Protein fractions were analyzed using Laemmli 12% SDS-PAGE. The gel was stained with EZblue protein stain (Sigma-Aldrich, USA) according to the manufacturer's protocol.

ItaT expression and purification. *Escherichia coli* BL21(DE3) cells harboring pET-his-*itaRT* were grown in LB media to an OD_{600} of 0.8, and induced with 1 mM IPTG for 16 h at 18°C. Cells were harvested by centrifugation and lysed by sonication in 50 ml of lysis buffer (50 mM Tris–HCl pH 7.5, 500 mM NaCl, 0.5 mM PMSF). The lysate clarified by centrifugation was incubated with 1 ml of Talon CellThru Co^{2+}-chelating resin (Takara-Clontech) with agitation for 3 h at 4°C. The resin was washed with 100 ml of wash buffer (50 mM Tris–HCl, pH 7.5; 500 mM NaCl, 10 mM imidazole) and the ItaRT complex anchored at the resin by 6xHis-tagged ItaR was treated with 10 ml of denaturing buffer (50 mM Tris–HCl pH 7.5, 500 mM NaCl, 5 M guanidine-HCl). The denatured ItaT dissociated from the ItaRT complex was separated from the resin and refolded by dialysis at 4°C for 16 h in 2 L of

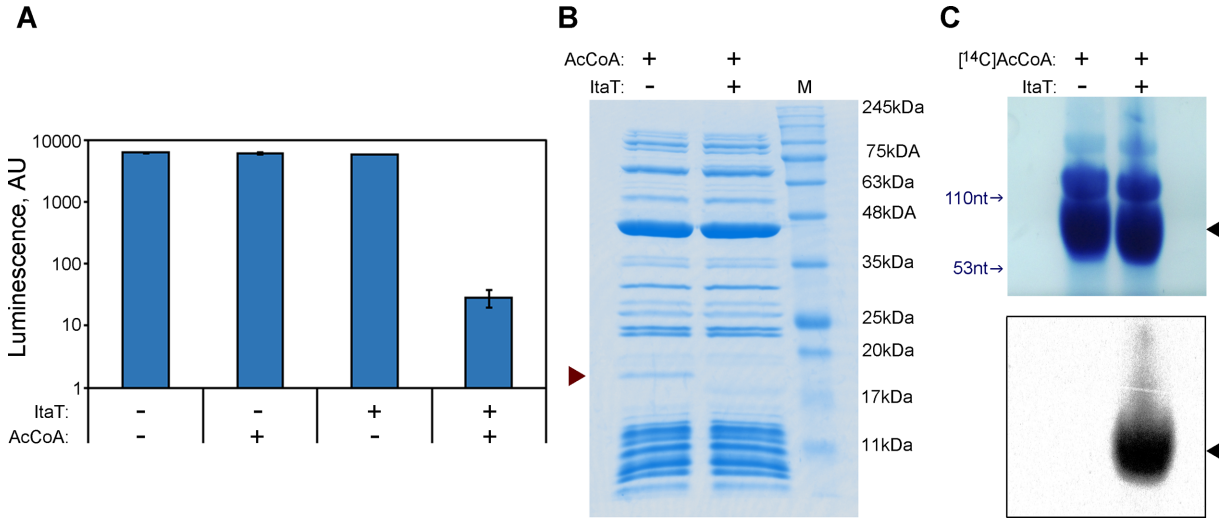

Figure 4. ItaT inhibits translation by acetylation of tRNA. (**A**) Activity of firefly luciferase synthesized in *in vitro* coupled transcription-translation PURExpress system in the absence or presence of ItaT, acetyl-CoA (AcCoA) or both. The graph shows the relative luminescence of samples obtained from three independent experiments expressed in arbitrary units, AU. The error bars represent standard deviation. (**B**) SDS-PAGE analysis of DHFR produced in the transcription-translation reaction described in (A). Reactions were supplemented with [^{14}C] acetyl-CoA and carried out in the absence (left) or presence of ItaT (right). Reaction products were visualized with Coomassie blue staining. The position of the DHFR protein band is indicated by the red arrowhead on the left. Lane M shows the molecular weight markers. (**C**) Analysis of tRNAs extracted from the samples shown in (B) by acid-urea PAGE followed by methylene blue staining (top panel) and autoradiography (lower panel). The position of tRNAs on the gel is indicated by the black arrowhead on the right.

dialysis buffer (25 mM Tris–HCl, pH 7.5; 25 mM NaCl, 1 mM DTT, 5% glycerol). Ca. 50% of ItaT remained soluble after dialysis, the rest precipitated and was discarded. The concentration of soluble ItaT was determined by Bradford method. ItaT was flash-frozen and stored at −80°C.

Asp-RS and Ile-RS purification. *Escherichia coli* JW0024 and JW1855 strains from ASKA collection (25) were used for Ile-RS and Asp-RS purification, respectively. Cells were grown in 250 ml of LB medium containing chloramphenicol (34 μg/ml) at 37 °C to OD_{600} = 0.6 followed by 2 h-induction with 1 mM IPTG. The induced cells were collected by centrifugation, sonicated in 5 ml of BW buffer supplemented with 0.2 mM PMSF, 1 mg/ml lysozyme and 1 mM β-mercaptoethanol. The His-tagged Ile-RS and Asp-RS were purified using HiTrap Co^{2+}-chelating HP Sepharose column (GE Healthcare). Proteins were eluted with EB buffer and applied on MonoQ 5/50 GL (GE Healthcare) column pre-equilibrated with Buffer A (20 mM HEPES pH 6.8, 50 mM NaCl) and eluted using the linear gradient of NaCl (from 50 to 500 mM) in the same buffer. Protein concentration was determined by Bradford method.

In vitro translation and toeprinting assays

The in vitro coupled transcription-translation reactions were carried out by PURExpress kit (NEB, USA) using DNA templates encoding the dihydrofolate reductase (DHFR) (NEB, USA) or the firefly luciferase (Promega, USA). Before template addition, translation reactions were incubated for 10 min at 37°C in the presence of 0.2 mM of cold acetyl coenzyme A (AcCoA) or radiolabeled [acetyl-1-^{14}C]-AcCoA (0.2 μCi, 60 mCi/mmol), Perkin Elmer, USA), with and without 2 μM ItaT. The enzymatic activity of *in vitro* synthesized luciferase was measured using the Steady-Glo Luciferase Assay System (Promega, USA). The products of DHFR *in vitro* translation reactions were analyzed by SDS-PAGE or by 12% denaturing acid-urea PAGE followed by autoradiography (12).

The DNA templates for *in vitro* translation of the wild-type and isoleucine-containing *yncJ* mutants were prepared by PCR of *E. coli* MG1655 genomic DNA using a reverse primer yncJ_NV1_R and one of the forward primers: yncJ_WT_F, yncJ_atc_F or yncJ_ata_F. The PCR products were converted to mRNA using T7Megascript *in vitro* transcription kit (Ambion, USA). *In vitro* translation reactions were carried out as described above except that the reaction mixture was supplemented with 0.5 μCi of L-[^{14}C]-valine (Perkin Elmer, USA). The reaction products were analyzed by SDS–PAGE followed by autoradiography.

The toeprinting assay was carried out using Rst1 and Rst2 mRNA as templates as described in (26), except that reactions were preincubated for 10 min with 0.4 mM AcCoA with or without the addition of 2 μM ItaT.

In vitro aminoacylation, acetylation and RNaseT1 treatment

The aminoacylation of the $tRNA^{Ile}_{s}$(GAU) and $tRNA^{Asp}$ (Subriden RNA, Rollingbay, WA, USA) was performed in 20 μl of reaction buffer (9 mM Mg-acetate, 5 mM KH_2PO_4 (pH 7.3), 95 mM K-glutamate, 5 mM NH_4Cl, 0.5 mM $CaCl_2$, 1 mM spermidine, 8 mM putrescine, 1 mM DTT) supplemented with 5 mM ATP, 0.5 mM of aspartate or isoleucine, 1 μl of corresponding aminoacyl tRNA synthetase and 3 μg of the tRNA. The reaction mixture was incubated at 37°C for 30 min followed by the addition of 0.4 mM AcCoA and 2 μM ItaT with subsequent incubation at 37°C for 10 min. 3μl of the reaction mixture was treated with 1U RNase T1 (NEB, USA) for 30 min. For acetylation

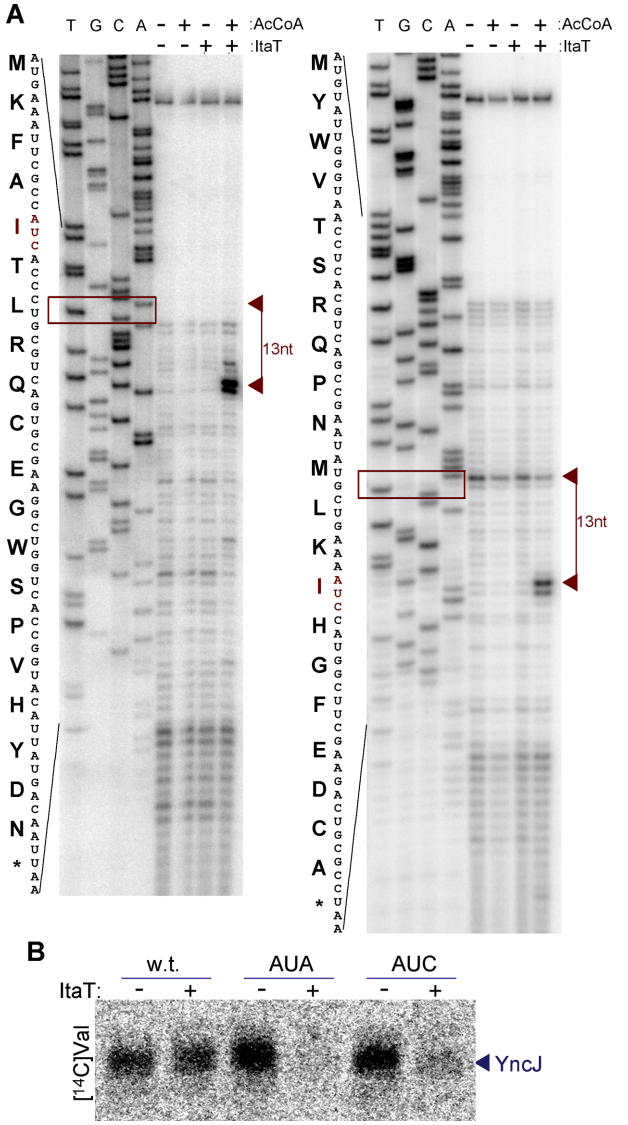

Figure 5. ItaT blocks translation on Ile codons in the presence of acetyl-CoA. (**A**) mRNA toeprint assay of ItaT specificity. Two DNA templates coding for 20- and 21-amino acid-long peptides (left and right panels, respectively) each containing codons for all 20 amino acids were used in *in vitro* transcription-translation assay (same as in Figure 3B) followed by reverse-transcription reaction. Samples were separated by denaturing urea-PAGE along with the DNA-sequencing markers (four leftmost lanes in each gel) and visualized by autoradiography. Specific bands that are present in the reactions containing both ItaT and acetyl-CoA but absent in the control samples correspond to codon-specific translation arrest. The peptide and corresponding mRNA sequences are shown on the left side of each panel. Positions on mRNA where reverse transcription is terminated due to the presence of stalled ribosome (toeprints) are indicated with red arrowheads. Codons located in the A-site of the stalled ribosome are marked by open red boxes. Note that owing to the large size of the ribosome, the reverse transcriptase stops at nucleotide +13 relative to the first base of mRNA codon located in the A site (38). (**B**) *In vitro* translation assay of the wild-type *yncJ* mRNA (w.t.) and its variants carrying alternative isoleucine codons (AUA and AUC). Reactions were supplemented with acetyl-CoA and [^{14}C]-valine and carried out in the presence or absence of ItaT, as indicated above the lanes. Radiolabeled reaction products were separated by SDS-PAGE and visualized by autoradiography and Phosphorimager. The position of bands, corresponding to the full-length YncJ is indicated by a blue arrowhead.

site identification charged acetylated tRNA^{Ile} was treated with 1 μg/ml RNase A in water at RT for 5 min.

Mass spectrometry

MALDI-TOF MS analysis was performed on UltrafleXetreme MALDI-TOF/TOF mass spectrometer (Bruker Daltonik, Germany) equipped with Nd laser. Samples for analysis were prepared as described (27). The MH+ of ItaR protein was measured in a linear mode; the accuracy of average mass peak measurement was within 1 Da. The MH+ molecular ions of RNase T1-treated tRNAs were measured in reflector mode; the accuracy of monoisotopic mass peak measurement was within 30 ppm. Fragmentation spectra were obtained in LIFT mode, the accuracy of daughter ions measurement was within 1 Da range. Mass-spectra were processed using FlexAnalysis 3.2 software (Bruker Daltonik, Germany) and analyzed manually.

GNAT sequence analysis

A full set of 4961 completely sequenced prokaryotic genomes was downloaded from the NCBI GenBank database (28) in March 2016 and annotated using PSI-BLAST (29) with CDD profiles (30). Proteins, matching one of the 16 GNAT profiles in CDD as well as those, not annotated identified with CDD, but identified using PSI-BLAST searches with known GNAT representatives as queries were filtered to remove multidomain proteins, resulting in the set of 96 453 GNAT sequences. The same procedure initiated with 46 antitoxin profiles and a set of known antitoxins produced a list of 98 182 predicted antitoxin sequences. Using this information all GNAT genes were classified into two groups: 2286 GNATs that are adjacent to antitoxins in the genomes and the remaining 94 167 GNATs.

Both sets of GNAT sequences were clustered using UCLUST (31) with the similarity threshold of 0.9; one representative of each cluster was selected for the further analysis (37,902 distinct sequences). The set of representatives was clustered using UCLUST with the similarity threshold of 0.5; sequences within a cluster were aligned using MUSCLE (32); singletons were added to the set of clusters as pseudo-alignments.

GNAT sequence clusters were further classified as follows: PSI-BLAST searches with GNAT alignments used as PSSMs were performed against the database, consisting of cluster consensus sequences. PSI-BLAST scores were converted into distances using the $d_{A,B} = -\ln(s_{A,B}/\min(s_{A,A},s_{B,B}))$ formula, where $d_{A,B}$ is the distance between cluster A and B and $s_{A,B}$ is the PSI-BLAST score for the comparison of these clusters. UPGMA tree was constructed from the distance matrix and cut at distance 1 from the leaves, forming clusters of clusters (superclusters). Superclusters, not containing any antitoxin-associated GNATs, were excluded from further analysis, resulting in the set of 24 454 sequences.

This set was further aligned using the following iterative procedure. All cluster alignments (including pseudo-alignments of singleton sequences) were compared to each other using HHSEARCH (32); HHSEARCH similarity

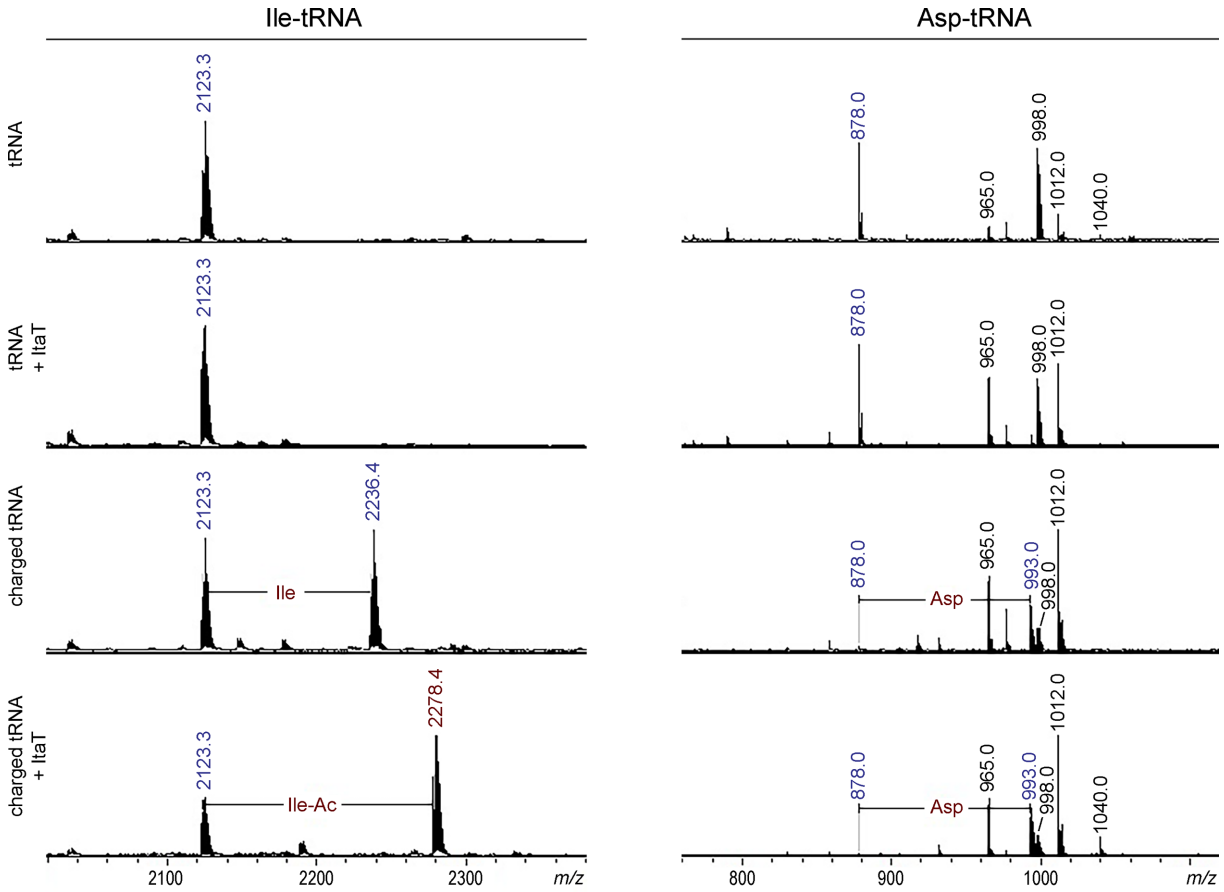

Figure 6. ItaT specifically acetylates charged $tRNA^{Ile}$. MALDI-TOF MS spectra of RNase T1-treated tRNAs. Acetylation activity of ItaT was tested using the $tRNA^{Ile}$ (left panels) and control $tRNA^{Asp}$ (right panels). Uncharged tRNAs (top two panels) or charged tRNAs (bottom two panels) were analyzed before and after treatment with ItaT in the presence of acetyl-CoA, as indicated on the left. For specific peak description, see text. The *m/z* values for peaks corresponding to the 3′-terminal fragments of the uncharged or aminoacylated tRNAs are shown in blue. The *m/z* value of the peak corresponding to the 3′fragment of acetylated Ile-$tRNA^{Ile}$ is shown in red. Insets show the zoomed-in view of the mass peaks of the unmodified and acetylated fragments of the 3′-isoleucyl- $tRNA^{Ile}$ (5′-CCUACCA-3′-Ile).

scores were converted to distances as described above; UPGMA trees were reconstructed from the pairwise distance matrices; tips of the UPGMA tree were used to guide progressive pairwise alignment of clusters using HHALIGN (33).

After the final iteration, the resulting alignments were filtered for positions containing over 50% of gaps and used to reconstruct approximate maximum likelihood trees using FastTree (34) (WAG evolutionary model, gamma-distributed site rates). The trees were rooted using a variant of the midpoint root procedure and combined into a single tree according to the UPGMA tree from the last round of the inter-cluster comparisons.

RESULTS

The *itaT* and *itaR E. coli* genes comprise a toxin–antitoxin system

The *Escherichia coli* HS genome (locus tag EcHs_A0501-EcHs_A0501) contains two partially overlapping genes, *itaR*, which encodes an 11.4-kDa protein containing an RHH DNA-binding domain characteristic of many type II antitoxins, and a downstream gene *itaT*, whose product is a 19.8-kDa GNAT family protein. The *itaRT* gene pair or *itaT* alone were cloned into a plasmid vector under control of an arabinose-inducible promoter. *Escherichia coli* MG1655 cells co-expressing *itaR* and *itaT* grew normally in the presence of arabinose. In contrast, the growth of cells expressing *itaT* alone was severely impaired under inducing conditions (Figure 1A), indicating that ItaT is toxic to cells. To test which major cellular process was affected by *itaT* expression the most, we performed metabolic pulse-labeling analysis of induced cells. As can be seen from Figure 1B, the effect on [^{3}H]-thymidine incorporation was minimal, [^{3}H]-uridine incorporation was modestly (30%) affected 10 min post-induction, while incorporation of [^{35}S]-methionine was affected strongly (80% inhibition) and the effect was evident 5 minutes post-induction. The results thus suggest that ItaT affects translation/protein synthesis.

To directly monitor cell fate upon *itaT* induction, we analyzed cells by live microscopy. Consistent with observed growth inhibition on agar plates (Figure 1A), the growth rate of cells harboring pBAD-*itaT* plasmid on arabinose-containing LB agarose blocks was dramatically lower than on glucose-containing medium (Supplementary Figure S1). Ninety minutes post-induction, only a small fraction of bac-

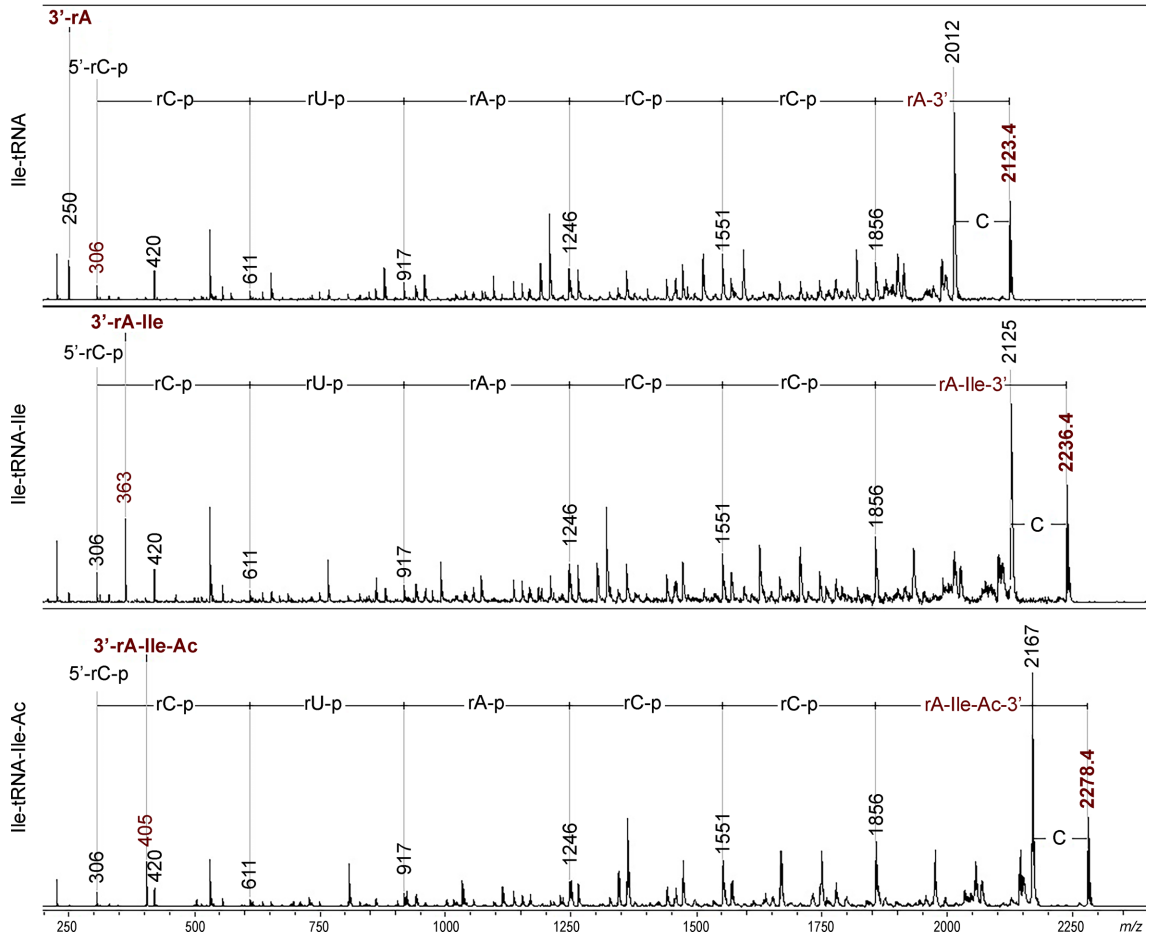

Figure 7. ItaT acetylates the 3′-terminal isoleucyl-adenosine in charged $tRNA^{Ile}$. Tandem MS–MS fragmentation spectra of the 3′-fragment of uncharged (top panel), Ile-charged (middle panel), and Ile-charged ItaT-acetylated (bottom panel) $tRNA^{Ile}$ fragments. The identity of ribonucleotides deduced from the spectra is indicated on top of each panel. The 3′-terminal isoleucyl-adenylate and N-acetyl-isoleucyl-adenylate fragments and their m/z values are shown in red. For detailed description of peaks, see text.

teria managed to finish a single cycle of cell division, while control cells transformed with an empty vector pBAD33 divided several times during this period (Figure 2). No visible changes in the shape of the *itaT*-expressing cells 90 min post-induction were observed, and their membranes appeared to remain intact. At longer post-induction times, cells expressing *itaT* but not the control cells were stained with propidium iodide (Figure 2), indicating that their membrane became compromised. To test if cells can recover from ItaT action, we induced them for 30 min and then transferred onto glucose-containing agarose blocks and observed them under the microscope. As can be seen from Supplementary Figure S2, most cells eventually became stained with propidium iodide and therefore were unable to recover. Yet, there was also a minor fraction of cells that after ∼100 min period of non-growth, started dividing, implying the existence of a detoxification mechanism.

Although GNAT family proteins show little identity in the primary structure, they possess a conserved fold (35). Structural alignment of ItaT homology-based model with the structures of Y145F KacT and Y148F TacT toxins (PDB ID: 5XUN, 5FVJ respectively) suggested that Y150 of ItaT could serve as a general acid that protonates the thiolate anion of CoA during the acetyl transfer reaction (35,36). A plasmid expressing ItaT*, an ItaT mutant carrying Y150A substitution, was constructed. Cells overproducing ItaT* grew normally (Figure 1A), indicating that toxicity of ItaT was abolished by the mutation.

The ItaRT complex is required for regulation of its own expression

Since the *itaT* toxicity was alleviated in the presence of *itaR* (Figure 1A), we tested whether ItaT and ItaR interact with each other. A plasmid co-expressing N-terminally Strep-tagged ItaR and C-terminally 6xHis-tagged ItaT was constructed. Extract of induced cells harboring such a plasmid was subjected to tandem affinity chromatography. Material from the Talon Co^{2+}-chelating resin to which 6xHis-tagged ItaT was expected to bind was subjected to the second round of purification on Strep-Tactin agarose. As can be seen from an SDS-PAGE presented in Figure 3A (lanes 1–7), the two proteins were eluted from this resin in apparently stoichiometric amounts (lane 7). The ItaRT* complex was also obtained (Figure 3A, lanes 8–14).

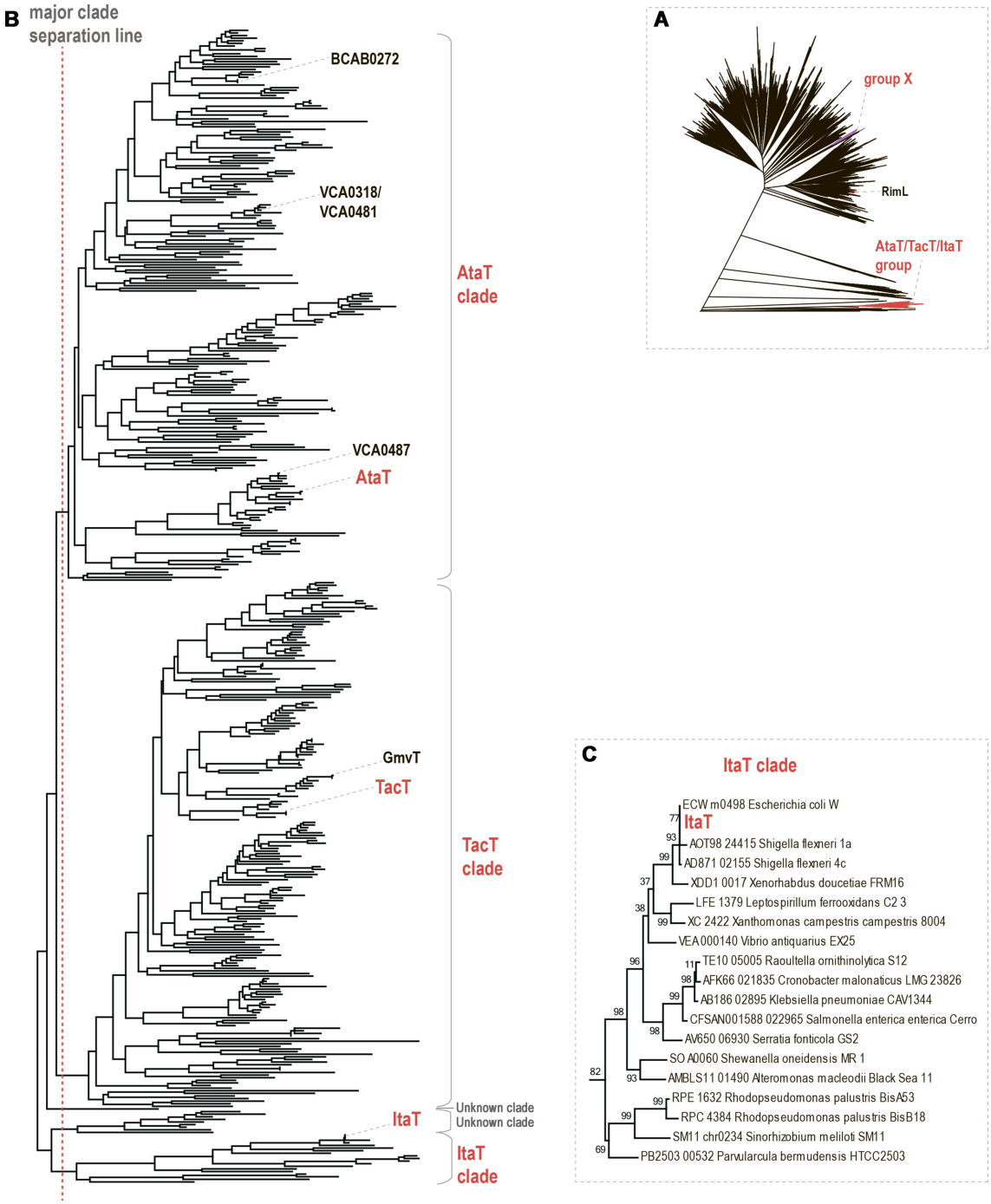

Figure 8. Classification and evolution of GNAT sequences. (**A**) Position of the AtaT/TacT/ItaT (red) and X (magenta) groups among other GNAT sequences. (**B**) Approximate maximum likelihood subtree of the AtaT/TacT/ItaT group is schematically shown on the left. Previously identified acetyltransferase toxins (17) are indicated. (**C**) Approximate maximum likelihood subtree of the ItaT clade. Support values calculated by the FASTTREE program are indicated for each branch.

The expression of Type II TA module genes is often controlled by the antitoxin and the toxin–antitoxin complex. Moreover, in the case of *tacAT*, which is related to *itaRT*, it was shown that the TacT toxin acetylates the TacA antitoxin, which increases the affinity of the complex to *tacAT* operon promoter (37). We tested whether ItaT can acetylate its cognate antitoxin ItaR. To this end, we measured the molecular mass of ItaR antitoxin from purified ItaRT and ItaRT* complexes by MALDI-TOF mass spectrometry (Supplementary Figure S3). In both samples antitoxin appeared as a single peak with an average [MH+] of 14512, matching the expected mass of ItaR with intact N-terminal affinity tag and removed N-terminal methionine residue. To test if the putative acetylating activity of ItaT is required for regulation of *itaRT* operon expression, we cloned the

172 bp-long upstream region of the *itaRT* operon containing a putative promoter into the pFD51 plasmid carrying promoterless *galK* gene (20). Cells harboring the resulting pFD-P_{itaRT}-*galK* fusion plasmid and compatible pBAD33 plasmids expressing *itaR*, *itaRT* or *itaRT** were induced with arabinose, total RNA was extracted, and levels of *galK* transcripts were measured by RT-qPCR (Figure 3B). Cells harboring pFD-P_{itaRT}-*galK* transcription fusion plasmid and empty pBAD33 vector had ∼40-fold higher levels of *galK* transcripts than cells carrying promoterless pFD51-*galK* control. Expression of *itaR* in the presence of either wild-type or mutant ItaT toxin decreased the amount of *galK* transcripts almost to background level. In contrast, expression of *itaR* alone had no effect. Thus, our data indicate that the ItaRT complex negatively regulates the *itaRT* expression, but this regulation is independent of the putative ItaT acetylating activity.

ItaT inhibits translation *in vitro* and acetylates tRNA

The ItaT action was next investigated *in vitro*. While the addition of recombinant ItaT or acetyl-CoA alone did not affect the synthesis of luciferase in an *in vitro* transcription-translation reaction, the simultaneous addition of ItaT and acetyl-CoA led to ∼200-fold decrease in luminescence (Figure 4A), in agreement with data obtained *in vivo* (Figure 1B).

To identify the target of ItaT, we performed *in vitro* translation of dihydrofolate reductase (DHFR) in PURExpress system in the presence of [^{14}C]-acetyl-CoA (Figure 4B). The production of DHFR was inhibited in the presence of purified ItaT, as judged by the absence of an ∼18 kDa band present in control reaction. Total RNA was next purified from *in vitro* translation reactions, subjected to acid-urea PAGE and radioactively labeled products were revealed by autoradiography (Figure 4C). Previously, the same approach was used to demonstrate that TacT acetylates tRNA (11). As can be seen, reaction containing ItaT and [^{14}C]-acetyl-CoA but not the control reaction lacking ItaT contained radioactively labeled tRNA, suggesting that ItaT inhibits translation by means of tRNA acetylation.

ItaT prevents translation of isoleucine codons

To reveal a specific effect of ItaT on protein synthesis, a toeprinting experiment was performed with mRNA containing an engineered short ORF harboring codons for each of the 20 amino acids (26). Stalling of a ribosome at a particular codon of the template manifests itself in the accumulation of primer extension products that arise due to the inability of reverse transcriptase to dislodge the ribosome (38). In the absence of ribosome stalling, most primers are elongated to the 5′ end of mRNA. As can be seen from Figure 5A, left, a strong stalling site was observed in reactions containing ItaT and acetyl-CoA. Mapping of the stall site indicates that it must have arisen due to ribosome stalling at the isoleucine AUC codon in the A-site, which is the fifth codon in the template used. To understand if the toeprint induced by ItaT is position-specific or is determined by the nature of the codon, toeprinting experiment was repeated with an alternative mRNA template where the AUC codon was located at position 14. As can be seen from Figure 5A, right, the position of ItaT-acetyl-CoA induced toeprint was moved further downstream on this template and corresponded to ribosome stalling at the Ile^{14} codon. The results thus suggest that ItaT induces specific stalling at isoleucine codons, rather than stalling at a particular distance from the translation start site.

In Bacteria, the isoleucine residue is encoded by three codons: AUU, AUC, and AUA. Two of these codons, AUU and AUC, are recognized by Ile-tRNA(GAU), while rare AUA codon is decoded by minor Ile-tRNA(k^2CAU) (39,40). To further address the issue of ItaT specificity, we made use of *E. coli yncJ*, a short ORF, which codes for an 8.7 kDa protein of unknown function. The YncJ sequence lacks isoleucine residues, while the other 19 amino acids are present. *In vitro* translation of the *yncJ* mRNA was performed in the presence or the absence of acetyl-CoA and ItaT. As can be seen from Figure 5B, ItaT had no effect on the accumulation of wild-type YncJ. To determine if ItaT can inactivate both Ile-tRNA(k^2CAU) and Ile-tRNA(GAU), we created two versions of the *yncJ* gene harboring either the AUC codon or the AUA codon at position 2. *In vitro* translation of the mutant *yncJ* mRNAs in the presence or the absence of acetyl-CoA and ItaT was next performed (Figure 5B). The synthesis of both isoleucine-containing YncJ variants was inhibited by ItaT and acetyl-CoA. The result thus suggests that the aminoacyl part of tRNA rather than tRNA itself is the major determinant of ItaT specificity.

ItaT acetylates the aminoacyl-adenosine moiety of charged $tRNA^{Ile}$

We next sought to map the ItaT acetylation site. $tRNA^{Ile}$ and control $tRNA^{Asp}$ were aminoacylated *in vitro* using cognate aminoacyl-tRNA synthetases. Both uncharged and charged tRNAs were treated with ItaT in the presence of acetyl-CoA. The tRNAs were then treated with RNase T1, which cleaves single-stranded RNA 3′ after guanine residues, and the products were analyzed using MALDI mass spectrometry. RNase T1 treatment results in the production of an m/z = 2123.3 3′-terminal fragment of Ile-tRNA(GAU), 5′-CCUACCA-3′, which is partially converted to an m/z = 2236.3 mass-ion after aminoacylation with isoleucine. In the case of $tRNA^{Asp}$, the 3′-terminal fragment 5′-CCA-3′ with m/z = 878 is converted to an m/z = 993 mass-ion by aminoacylation with cognate amino acid. Treatment of uncharged $tRNA^{Ile}$, $tRNA^{Asp}$ or aminoacylated Asp-$tRNA^{Asp}$ with ItaT and acetyl-CoA did not lead to alterations of their mass-spectra (Figure 6). In contrast, charged Ile-$tRNA^{Ile}$ incubation with ItaT and acetyl-CoA resulted in the appearance of an additional m/z = 2278.4 mass-ion. The 42 Da shift (from 2236.3 to 2278.4) is consistent with acetylation.

Tandem mass-spectrometry was next used to map the position of the acetyl group in the Ile-$tRNA^{Ile}$. Comparative analysis of fragmentation spectra of 2123.4, 2236.4 and 2278.4 mass-ions revealed the presence of an m/z = 363 peak matching the 3′-terminal riboadenosine charged with Ile in the spectrum of ItaT-untreated reaction. No such peak was observed in the spectrum of the ItaT-treated

sample. Instead, an $m/z = 405$ mass-ion matching the 3′-terminal riboadenosine charged with acetylated Ile was detected (Figure 7). Mass peaks corresponding to the 3′-fragment 3′CCUACC-5′ of tRNA were present in all spectra. Taken together, we conclude that ItaT specifically modifies charged $tRNA^{Ile}$ and the acetyl group is located at the 3′-isoleucyl-adenosine.

To locate further the acetyl group, acetylated Ile-$tRNA^{Ile}$ was digested with RNase A and the 3′-terminal modified adenosine (m/z 423.3) was subjected to MS-MS analysis (Supplementary Figure S3). Daughter peaks with m/z 136 and m/z 156, matching intact adenine moiety and acetylated isoleucine were observed. We conclude that the acetyl group is attached to the isoleucine residue.

DISCUSSION

In this work, we establish that ItaT is a type II toxin that inhibits translation by acetylating Ile-$tRNA^{Ile}$. Though the *itaRT* gene pair was identified in the natural *E. coli* HS isolate, a virtually identical gene pair is encoded in the common laboratory strain *E. coli* BL21(DE3) (locus tags ECD_00377-ECD_00378). As is the case with many other TA modules, the functional significance of *itaRT* to its hosts, if any, is unknown. It is also not known which system may be responsible for reactivation and/or detoxification of ItaT-modified aminocylated $tRNA^{Ile}$. Likely candidates are the broad-spectrum deacetylase CobB or peptidyl-tRNA hydrolase Pth (11).

ItaT is a novel type II toxin shown to selectively acetylate specific elongator tRNA. Several other proteins belonging to the GNAT family have been shown to be toxic when overexpressed and/or inhibit translation (17). GNATs are highly diverse superfamily of proteins performing various functions in the cell. Substrates for acetylation range from small molecules to proteins and RNA (41). We performed a phylogenetic analysis of GNAT proteins encoded in genomes of prokaryotes. 779 distinct acetyltransferases are encoded next to a gene encoding an identifiable type II antitoxin, thus forming putative toxin–antitoxin pairs. The phylogenetic tree shows that all experimentally confirmed toxin acetyltransferases are monophyletic, forming a compact branch, distant from other groups of acetyltransferases (Figure 8A). We named this group the 'TacT/AtaT/ItaT group'. TacT/AtaT/ItaT group is very distinct from the rest of acetyltransferases and covers about 1% of the whole diversity of GNATs. These sequences are present in 11 bacterial phyla and are quite abundant in some of them (e.g. in Proteobacteria, where they are identified in 54 out of 121 families). Most of these genes are encoded in genomes next to a predicted antitoxin, suggesting that these proteins are deeply specialized in their roles of toxins in toxin–antitoxin pairs, presumably as a part of controlled cell death or stress-resistance systems.

Close examination of the TacT/AtaT/ItaT group identified five clades potentially corresponding to different specificities of respective toxins (Figure 8B). One clade includes AtaT and may comprise acetyltransferases targeting methionine moiety on initiator Met-$tRNA^{fMet}$. TacT is present in another clade whose members may include acetyltransferases targeting amino group of various elongator aminoacyl-tRNAs, and thus have relaxed specificity. Members of the clade that contains ItaT (Figure 8C) may acetylate elongator Ile-$tRNA^{Ile}$. The remaining two clades contain no validated members and may include acetyltransferases with additional specificities.

There is only one other large GNAT family tree branch indicated as group X enriched with acetyltransferases encoded next to potential antitoxins (Figure 8A). In contrast to the extended TacT/AtaT/ItaT group that is very distantly related to other GNATs, group X is relatively small (297 distinct sequences or ∼0.8% of the whole diversity) and forms a branch on a periphery of a huge family, containing the majority of acetyltransferases. GNATs of group X are part of two-protein systems: one being the acetyltransferase and another—an Xre-HTH family domain fused to a cupin domain. The latter combination of domains is often found as a component of various oxidoreductases, but its specific function is not known.

The TacT/AtaT/ItaT and X groups together cover about 50% of acetyltransferases that are ever found encoded next to antitoxin-like transcriptional regulators. The rest, however, are spread across the tree and do not form coherent clades.

If the TA modules with acetylating toxins are primarily functioning as selfish and addictive elements, it can be expected that they will be forced to diversify their target specificity, as is common, for example, for restriction-modification systems (42). In this case, one can expect non-overlapping specificities even for members of the same clade, perhaps extending to all twenty aminoacyl-tRNA synthetases. It is worth noting in this respect that GNAT acetyltransferases MccE acetylate aminoacid moieties of toxic aminoacyl nucleotides and have complex non-overlapping specificities that depend on the nature of both the nucleotide and amino acid and may be additionally affected by tailoring modifications (27,43). Closely related acetyltransferase RimL, responsible for L12 ribosomal protein acetylation, also contributes to the protection of bacteria from toxic aminoacyl nucleotides by acetylating the aminoacyl moiety (44). Possible evolution of TA systems from systems of resistance to antibiotics is consistent with the idea of TA systems functioning as 'anti-addiction modules' (45), useful parasites protecting bacteria from other parasites.

Investigation of aminoacyl-tRNA acetylating toxins is still in its infancy. Our study contributed to the characterization of specificity of such toxins towards particular tRNA species. Further experimental validation of predicted TA modules of this kind and investigation of specificities of their toxins is currently ongoing in our laboratories.

SUPPLEMENTARY DATA

Supplementary Data are available at NAR Online.

FUNDING

Skoltech; Russian Science Foundation [16-14-10356 to S.D.]; Toe-printing, *in vitro* translation of luciferase, YncJ mutant creation and *in vitro* translation experiments were supported by Russian Science Foundation [17-75-30027 to

P.S.]; intramural funds of the US Department of Health and Human Services (to National Library of Medicine) (to K.S.M., Y.I.W.); intramural funds of the Department of Cell Biology and Neuroscience and the Graduate School of Biomedical Studies at Rowan University (to S.B.). BG and SH were supported by an MRC Career Development Award MR/M009629/1 to S.H. Funding for open access charge: Skoltech.
Conflict of interest statement. None declared.

REFERENCES

1. Makarova,K.S, Wolf,Y.I. and Koonin,E.V. (2013) Comparative genomics of defense systems in archaea and bacteria. *Nucleic Acids Res.*, **41**, 4360–4377.
2. Hayes,F. and Van Melderen,L. (2011) Toxins-antitoxins: diversity, evolution and function. *Crit. Rev. Biochem. Mol. Biol.*, **46**, 386–408.
3. Page,R. and Peti,W. (2016) Toxin–antitoxin systems in bacterial growth arrest and persistence. *Nat. Chem. Biol.*, **12**, 208–214.
4. Muthuramalingam,M., White,J.C. and Bourne,C.R. (2016) Toxin–antitoxin modules are pliable switches activated by multiple protease pathways. *Toxins (Basel)*, **8**, 214.
5. Van Melderen,L. and Saavedra De Bast,M. (2009) Bacterial toxin–antitoxin systems: more than selfish entities? *PLoS Genet.*, **5**, e1000437.
6. Dy,R.L., Richter,C., Salmond,G.P. and Fineran,P.C. (2014) Remarkable mechanisms in microbes to resist phage infections. *Annu. Rev. Virol.*, **1**, 307–331.
7. Lobato-Márquez,D., Díaz-Orejas,R. and García-Del Portillo,F. (2016) Toxin–antitoxins and bacterial virulence. *FEMS Microbiol. Rev.*, **40**, 592–609.
8. Hall,A.M., Gollan,B. and Helaine,S. (2017) Toxin–antitoxin systems: reversible toxicity. *Curr. Opin. Microbiol.*, **36**, 102–110.
9. Harms,A., Brodersen,D.E., Mitarai,N. and Gerdes,K. (2018) Toxins, targets, and triggers: an overview of toxin–antitoxin biology. *Mol. Cell*, **70**, 768–784.
10. Makarova,K.S., Wolf,Y.I. and Koonin,E.V. (2009) Comprehensive comparative-genomic analysis of type 2 toxin–antitoxin systems and related mobile stress response systems in prokaryotes. *Biol. Direct.*, **4**, 19.
11. Leplae,R., Geeraerts,D., Hallez,R., Guglielmini,J., Drèze,P. and Van Melderen,L. (2011) Diversity of bacterial type II toxin–antitoxin systems: a comprehensive search and functional analysis of novel families. *Nucleic Acids Res.*, **39**, 5513–5525.
12. Cheverton,A.M., Gollan,B., Przydacz,M., Wong,C.T., Mylona,A., Hare,S.A. and Helaine,S. (2016) A Salmonella toxin promotes persister formation through acetylation of tRNA. *Mol. Cell.*, **63**, 86–96.
13. Rycroft,J.A., Gollan,B., Grabe,G.J., Hall,A., Cheverton,A.M., Larrouy-Maumus,G., Hareand,S.A. and Helaine,S. (2018) Activity of acetyltransferase toxins involved in Salmonella persister formation during macrophage infection. *Nat. Commun.*, **9**, 1993.
14. Jurėnas,D., Chatterjee,S., Konijnenberg,A., Sobott,F., Droogmans,L., Garcia-Pino,A. and Van Melderen,L. (2017) AtaT blocks translation initiation by N-acetylation of the initiator tRNA(fMet). *Nat. Chem. Biol.*, **13**, 640–646.
15. Van Melderen,L., Jurenas,D. and Garcia-Pino,A. (2017) Messing up translation from the start: How AtaT inhibits translation initiation in E. coli. *RNA Biol.*, **3**, 1–5.
16. McVicker,G. and Tang,C.M. (2016) Deletion of toxin–antitoxin systems in the evolution of Shigella sonnei as a host-adapted pathogen. *Nat. Microbiol.*, **2**, 16204.
17. Jurėna,D., Garcia-Pino,A. and Van Melderen,L. (2017) Novel toxins from type II toxin–antitoxin systems with acetyltransferase activity. *Plasmid*, **93**, 30–35.
18. Van Acker,H., Sass,A., Dhondt,I., Nelis,H.J. and Coenye,T. (2014) Involvement of toxin–antitoxin modules in Burkholderia cenocepacia biofilm persistence. *Pathog. Dis.*, **71**, 326–335.
19. Iqbal,N., Guérout,A.M., Krin,E., Le Roux,F. and Mazel,D. (2015) Comprehensive functional analysis of the 18 Vibrio cholerae N16961 toxin–antitoxin systems substantiates their role in stabilizing the superintegron. *J. Bacteriol.*, **197**, 2150–2159.
20. Qian,H., Yao,Q., Tai,C., Deng,Z., Gan,J. and Ou,H.Y. (2018) Identification and characterization of acetyltransferase-type toxin–antitoxin locus in *Klebsiella pneumoniae*. *Mol. Microbiol.*, **108**, 336–349.
21. Ho,S.N., Hunt,H.D., Horton,R.M., Pullen,J.K. and Pease,L.R. (1989) Site-directed mutagenesis by overlap extension using the polymerase chain reaction. *Gene*, **77**, 51–59.
22. Rak,B. and von Reutern,M. (1984) Insertion element IS5 contains a third gene. *EMBO J.*, **3**, 807–811.
23. Strotskaya,A., Savitskaya,E., Metlitskaya,A., Morozova,N., Datsenko,K.A., Semenova,E. and Severinov,K. (2017) The action of Escherichia coli CRISPR-Cas system on lytic bacteriophages with different lifestyles and development strategies. *Nucleic Acids Res.*, **45**, 1946–1957.
24. Schneider,C.A., Rasband,W.S. and Eliceiri,K.W. (2012) NIH Image to ImageJ: 25 years of image analysis. *Nat. Methods.*, **9**, 671–675.
25. Kitagawa,M., Ara,T., Arifuzzaman,M., Ioka-Nakamichi,T., Inamoto,E., Toyonaga,H. and Mori,H. (2005) Complete set of ORF clones of Escherichia coli ASKA library (a complete set of E. coli K-12 ORF archive): unique resources for biological research. *DNA Res.*, **12**, 291–299.
26. Orelle,C., Szal,T., Klepacki,D., Shaw,K.J., Vázquez-Laslop,N. and Mankin,A.S. (2013) Identifying the targets of aminoacyl-tRNA synthetase inhibitors by primer extension inhibition. *Nucleic Acids Res.*, **41**, e144.
27. Serebryakova,M., Tsibulskaya,D., Mokina,O., Kulikovsky,A., Nautiyal,M., Van Aerschot,A., Severinov,K. and Dubiley,S. (2016) A Trojan-horse peptide-carboxymethyl-cytidine antibiotic from Bacillus amyloliquefaciens. *J. Am. Chem. Soc.*, **138**, 15690–15698.
28. Benson,D.A., Cavanaugh,M., Clark,K., Karsch-Mizrachi,I., Ostell,J., Pruitt,K.D. and Sayers,E.W. (2018) GenBank. *Nucleic Acids Res.*, **46**, D41–D47.
29. Altschul,S.F., Madden,T.L., Schäffer,A.A., Zhang,J., Zhang,Z., Miller,W. and Lipman,D.J. (1997) Gapped BLAST and PSI-BLAST: a new generation of protein database search programs. *Nucleic Acids Res.*, **25**, 3389–3402.
30. Marchler-Bauer,A., Derbyshire,M.K., Gonzales,N.R., Lu,S., Chitsaz,F., Geer,L.Y., Geer,R.C., He,J., Gwadz,M., Hurwitz,D.I. *et al.* (2015) CDD: NCBI's conserved domain database. *Nucleic Acids Res.*, **43**, D222–D226.
31. Edgar,R.C. (2010) Search and clustering orders of magnitude faster than BLAST. *Bioinformatics*, **26**, 2460–2461.
32. Edgar,R.C. (2004) MUSCLE: a multiple sequence alignment method with reduced time and space complexity. *BMC Bioinformatics*, **5**, 113.
33. Söding,J. (2005) Protein homology detection by HMM-HMM comparison. *Bioinformatics*, **21**, 951–960.
34. Price,M.N., Dehal,P.S. and Arkin,A.P. (2010) FastTree 2–approximately maximum-likelihood trees for large alignments. *PLoS One*, **5**, e9490.
35. Vetting,M.W, S de Carvalho,L.P, Yu,M., Hegde,S.S., Magnet,S., Roderick,S.L. and Blanchard,J.S. (2005) Structure and functions of the GNAT superfamily of acetyltransferases. *Arch. Biochem. Biophys.*, **433**, 212–226.
36. Salah Ud-Din,A.I., Tikhomirova,A. and Roujeinikova,A. (2016) Structure and functional diversity of GCN5-related N-acetyltransferases (GNAT). *Int. J. Mol. Sci.*, **17**, 1018.
37. VanDrisse,C.M., Parks,A.R. and Escalante-Semerena,J.C. (2017) A toxin involved in Salmonella persistence regulates its activity by acetylating its cognate antitoxin, a modification reversed by CobB sirtuin deacetylase. *MBio*, **8**, e00708-17.
38. Hartz,D., McPheeters,D.S., Traut,R. and Gold,L. (1998) Extension inhibition analysis of translation initiation complexes. *Methods Enzymol.*, **164**, 419–425.
39. Agris,P.F. (2004) Decoding the genome: a modified view. *Nucleic Acids Res.*, **32**, 223–238.
40. Muramatsu,T., Nishikawa,K., Nemoto,F., Kuchino,Y., Nishimura,S., Miyazawa,T. and Yokoyama,S. (1988) Codon and amino-acid specificities of a transfer RNA are both converted by a single post-transcriptional modification. *Nature*, **336**, 179–181.
41. Favrot,L., Blanchard,J.S. and Vergnolle,O. (2016) Bacterial GCN5-Related N-acetyltransferases: from resistance to regulation. *Biochemistry*, **55**, 989–1002.

42. Kusano,K., Naito,T., Handa,N. and Kobayashi,I. (1995) Restriction-modification systems as genomic parasites in competition for specific sequences. *Proc. Natl. Acad. Sci. U.S.A.*, **92**, 11095–11099.
43. Tsibulskaya,D., Mokina,O., Kulikovsky,A., Piskunova,J., Severinov,K., Serebryakova,M. and Dubiley,S. (2017) The product of Yersinia pseudotuberculosis mcc operon is a peptide-cytidine antibiotic activated inside producing cells by the TldD/E protease. *J. Am. Chem. Soc.*, **139**, 16178–16187.
44. Kazakov,T., Kuznedelov,K., Semenova,E., Mukhamedyarov,D., Datsenko,K.A., Metlitskaya,A., Vondenhoff,G.H., Tikhonov,A., Agarwal,V., Nair,S. *et al.* (2014) The RimL transacetylase provides resistance to translation inhibitor microcin C. *J. Bacteriol.*, **196**, 3377–3385.
45. Saavedra De Bast,M., Mine,N. and Van Melderen,L. (2008) Chromosomal toxin–antitoxin systems may act as antiaddiction modules. *J. Bacteriol.*, **190**, 4603–4609.